

# Robust large area molecular junctions of self-assembled monolayers of a model helical paddlewheel complex

Isabel Coloma,<sup>a</sup> Thierry Buffeteau,<sup>b</sup> Gilles Pecastaings,<sup>c</sup> Santiago Herrero,<sup>a,d</sup> Elizabeth Hillard,<sup>e</sup> Patrick Rosa,<sup>e</sup> Miguel Cortijo\*<sup>a</sup> and Mathieu Gonidec\*<sup>e</sup>

<sup>a</sup> MatMoPol Research Group, Inorganic Chemistry Department, Faculty of Chemical Sciences, Complutense University of Madrid, E-28040 Madrid, Spain.

<sup>b</sup> Univ. Bordeaux, CNRS, Bordeaux INP, ISM, UMR 5255, F-33405 Talence, France.

<sup>c</sup> Univ. Bordeaux, CNRS, CRPP, UMR 5031, F-33600 Pessac, France.

<sup>d</sup> Knowledge Technology Institute, Complutense University of Madrid, Campus de Somosaguas, 28223 Pozuelo de Alarcón, Madrid, Spain.

<sup>e</sup> Univ. Bordeaux, CNRS, Bordeaux INP, ICMCB, UMR 5026, F-33600 Pessac, France.

KEYWORDS: paddlewheel, diruthenium, chirality, helicity, self-assembled monolayers, molecular electronics

## Experimental part

**General materials and methods:** Solvents and reactants were obtained from commercial sources and were used as received, except for  $[\text{Ru}_2(\mu\text{-ap})_4\text{Cl}]$  (**RuapCl**), which was prepared as reported elsewhere.<sup>1</sup> The elemental analysis was performed by the Microanalytical Service of the Complutense University of Madrid. Electrospray ionization (ESI) mass spectrum was collected by the Mass Spectrometry Service of Complutense University of Madrid, using an ion trap-Bruker Esquire-LC spectrometer. The ATR spectrum was recorded with a ThermoScientific iS50 FTIR spectrometer, using a single-reflection ATR accessory (Specac) equipped with a germanium (Ge) crystal. The electronic spectrum of a  $\sim 10^{-5}$  M dichloromethane solution of the complex was recorded employing a Cary 5G spectrometer. Variable-temperature magnetization measurements were performed on a Quantum Design MPMSXL SQUID magnetometer. The data were corrected for the diamagnetic contribution to the susceptibility of the compound and the sample holder.

**Substrate preparation:** The template stripped Au<sup>TS</sup> substrates were prepared following a standard procedure<sup>2</sup> using a Korvus Technology HEX thermal evaporator to deposit the gold (200 nm) on a polished Si wafer without an adhesion layer, and glass chips were

glued to the gold film with photocurable NOA 61 optical adhesive (Norland). The classical gold substrates were prepared by depositing an adhesion layer of Cr (10nm) followed by a thicker film of Au (200 nm) using the same setup.

***Self-Assembled Monolayers (SAMs) preparation:*** The glass substrates and all the glassware (vials and syringes) were thoroughly cleaned with Hellmanex III special cleaning concentrate and milliQ water. The SAMs were prepared by incubating the substrates in a solution of roughly 0.1 mg of compound in 3 mL of toluene in closed brown vials purged with nitrogen. Upon removing the substrates from solution, the SAMs were rinsed with clean toluene and dried under a stream of nitrogen gas filtered through a 0.45 mm frit.

***Time of Flight Secondary Ion Mass Spectrometry (ToF-SIMS):*** The ToF-SIMS spectra were measured with a TOF.SIMS 5 spectrometer (IONTOF GmbH) equipped with a bismuth liquid metal ion gun (LMIG) oriented at 45° to the sample. The diameter of the LMIG 30 kV Bi<sup>3+</sup> ion beam was approximately 5 μm. The beam was operated at a 0.3 pA ion current in spectrometry mode and was raster scanned over the surface to generate 500 × 500 μm, 128 px × 128 px secondary ion images. Samples were grounded, and no charge effect was noticed during analysis. The total dose per image was kept below 10<sup>8</sup> ions cm<sup>-2</sup>.

***Polarization Modulation Infrared Reflection Absorption Spectroscopy (PM-IRRAS) and Attenuated Total Reflection (ATR):*** The PM-IRRAS spectrum of the SAM of [Ru<sub>2</sub>(μ-ap)<sub>4</sub>(NCS)] (**RuapNCS**) on gold was recorded on a ThermoNicolet Nexus 670 FTIR spectrometer at a resolution of 4 cm<sup>-1</sup>, by coadding eight blocks of 1500 scans (4 h total acquisition time). All spectra were collected in a dry-air atmosphere. Experiments were performed at an incidence angle of 75° using an external homemade goniometer reflection attachment.<sup>3</sup> The infrared parallel beam (modulated in intensity at frequency f<sub>i</sub> lower than 5 kHz) was directed out of the spectrometer with an optional flipper mirror and made slightly convergent with a first BaF<sub>2</sub> lens (191 mm focal length). The IR beam passed through a BaF<sub>2</sub> wire grid polarizer (Specac), to select the p-polarized radiation, and a ZnSe photoelastic modulator (PEM, Hinds Instruments, type II/ZS50). The PEM modulated the polarization of the beam at a high fixed frequency, 2f<sub>m</sub>=100 kHz, between the parallel and perpendicular linear states. After reflection on the sample, the double

modulated (in intensity and in polarization) infrared beam was focused with a second ZnSe lens (38.1 mm focal length) onto a photovoltaic MCT detector (Kolmar Technologies, Model KV104) cooled at 77 K. The polarization modulated signal  $I_{AC}$  was separated from the low frequency signal  $I_{DC}$  ( $f_i$  between 500 and 5000 Hz) with a 40 kHz high pass filter and then demodulated with a lock-in amplifier (Stanford Model SR 830). The output time constant was set to 1 ms. The two interferograms were high-pass and low-pass filtered (Stanford Model SR 650) and simultaneously sampled in the dual channel electronics of the spectrometer. In all experiments, the PEM was adjusted for a maximum efficiency at  $2500\text{ cm}^{-1}$  to cover the mid-IR range in only one spectrum. For calibration measurements, a second linear polarizer (oriented parallel or perpendicular to the first preceding the PEM) was inserted between the sample and the second ZnSe lens. This procedure was used to calibrate and convert the PM-IRRAS signal in terms of the IRRAS signal (i.e.,  $1 - R_p(d)/R_p(0)$ ) where  $R_p(d)$  and  $R_p(0)$  stand for the p-polarized reflectance of the film/substrate and bare substrate systems, respectively).<sup>4,5</sup>

The polarized ATR spectra of **RuapNCS** were recorded on a ThermoScientific iS50 FTIR spectrometer at a resolution of  $4\text{ cm}^{-1}$ , by coadding 500 scans. ATR experiments were performed using a single-reflection ATR accessory (Specac) equipped with a germanium (Ge) crystal and a DTGS detector. A  $\text{BaF}_2$  wire grid polarizer was added to record the spectra in the p- and s-polarizations. The film was obtained after evaporation of  $10\text{ }\mu\text{L}$  of a **RuapNCS** dichloromethane solution dropped onto the Ge crystal.

**Density Functional Theory (DFT) calculations:** DFT calculations were performed in gas-phase using the Gaussian 09 program.<sup>6</sup> The geometry was optimized at the B3LYP/LANL2DZ level. The vibrational spectra were computed and the frequencies were corrected using the tabulated empirical value for B3LYP/LANL2DZ of 0.9612 from the NIST CCCBDB database.<sup>7</sup>

**Atomic Force Microscopy (AFM):** The surface morphology of the SAMs was characterized with a Bruker Dimension Icon AFM in tapping mode, using NCHV antimony (n)-doped Si tips. The scan rate was 2 Hz on the Au substrate and 1 Hz on the SAM.

**Synthesis of  $[\text{Ru}_2(\mu\text{-ap})_4(\text{NCS})]$  (**RuapNCS**):** A solution of KSCN (3.50 mg, 0.04 mmol) in 6 mL of acetone was added over a solution of  $[\text{Ru}_2(\mu\text{-ap})_4\text{Cl}]$  (**RuapCl**) (30.00 mg, 0.03

mmol) in 6 mL of dichloromethane. The mixture was stirred overnight at room temperature in absence of light. The solution turned from green to yellow. The mixture was filtered through Celite® and the solution was taken to dryness. The resulting solid was redissolved in dichloromethane, filtered, and added to an extraction funnel. Then, it was washed with distilled water (2×15 mL), dried over magnesium sulfate and filtered. The solution was taken to dryness and the resulting solid was dissolved in cyclohexane and filtered. The solvent was evaporated obtaining a yellowish-brown solid. Yield: 92% (31.00 mg). Elemental analysis for  $C_{45}H_{36}N_9SRu_2 \cdot C_6H_{12} \cdot 0.5H_2O$  (1030.223  $g \cdot mol^{-1}$ ): % found (theoretical); 59.50 % C, (59.46); 4.71 % H, (4.79); 12.23 % N, (12.24); 3.29 % S (3.11). IR:  $\nu$  ( $cm^{-1}$ ) = 3055w, 3029w, 2024vs, 1900m, 1796w, 1730w, 1600s, 1587s, 1540m, 1464vs, 1447m, 1427vs, 1353s, 1284s, 1257m, 1216s, 1156s, 1114m, 1070m, 1017s, 999m, 951w, 917m, 861vs, 753vs, 734s, 696vs, 673s, 649m, 620w, 606m. UV/Vis-NIR ( $CH_2Cl_2$ ):  $\lambda_{max}$  ( $\epsilon / M^{-1} \cdot cm^{-1}$ ) = 267 (44600),  $\sim 325$  sh (21000),  $\sim 467$  sh (5700), 770 (5800) nm. MS (ESI<sup>+</sup>):  $m/z$  = 938.3 (100 %),  $[M]^+$ .

**Preparation of the SAMs of RuapNCS on Au and Au<sup>TS</sup>:** Self-assembled monolayers (SAMs) of **RuapNCS** were prepared on template-stripped gold (Au<sup>TS</sup>) for AFM and EGaln measurements and standard gold on silicon substrates for ToF-SIMS and PM-IRRAS analyses. The SAMs were obtained by incubation of the substrates in dilute solutions of the complex in toluene during 3.5 h at room temperature. Then, the samples were rinsed with clean solvent and dried under a filtered nitrogen stream, obtaining the desired SAMs Au<sup>TS</sup>-**RuapNCS** and Au-**RuapNCS**.

**Charge transport measurements:** Template-stripped gold was employed as the bottom-electrode and selected conical Ga<sub>2</sub>O<sub>3</sub>/EGaln tips as top-electrodes for charge transport measurements across the diruthenium SAM. A syringe loaded with the liquid metal Ga<sub>2</sub>O<sub>3</sub>/EGaln (see Figure S14) was used to form the tips by contact of a drop with a blank gold substrate. The formation of the tips was observed by optical microscopy. Once well formed, tips were approached to Au<sup>TS</sup>-**RuapNCS** in order to form contacts. Each tip was employed to form a unique junction Au<sup>TS</sup>-**RuapNCS**//Ga<sub>2</sub>O<sub>3</sub>/EGaln, and data collection consisted in 20 J-V cycles between  $\pm 0.5$  V starting at 0 V in 0.05 V increments.

## Supporting Figures

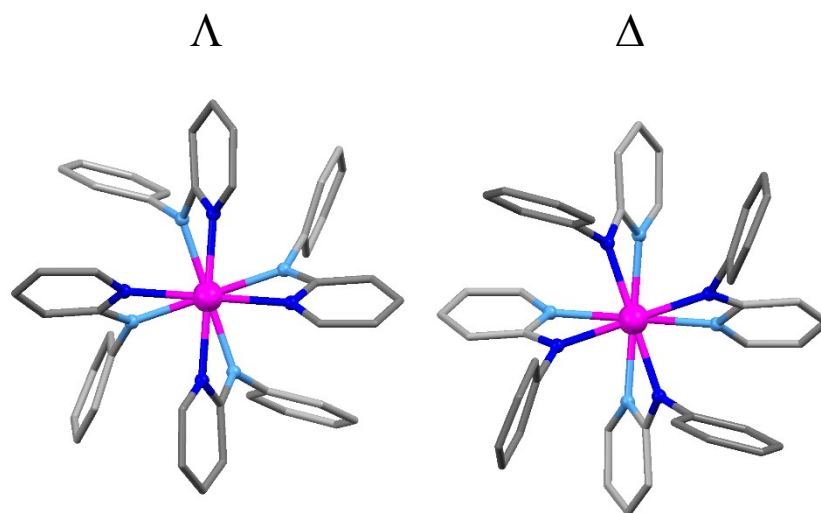


**Figure S1.** View of **RuapCl** along the M-M bond axis. Note that the crystal structure contains both lambda and delta enantiomers, from CUWWAS<sup>1</sup> found in the CSD database. Ru atoms are shown in pink, N atoms in blue and C atoms in grey. Cl and H atoms are omitted for clarity. N and C atoms located at the back are depicted in a lighter color for a better viewing of the helix configuration.

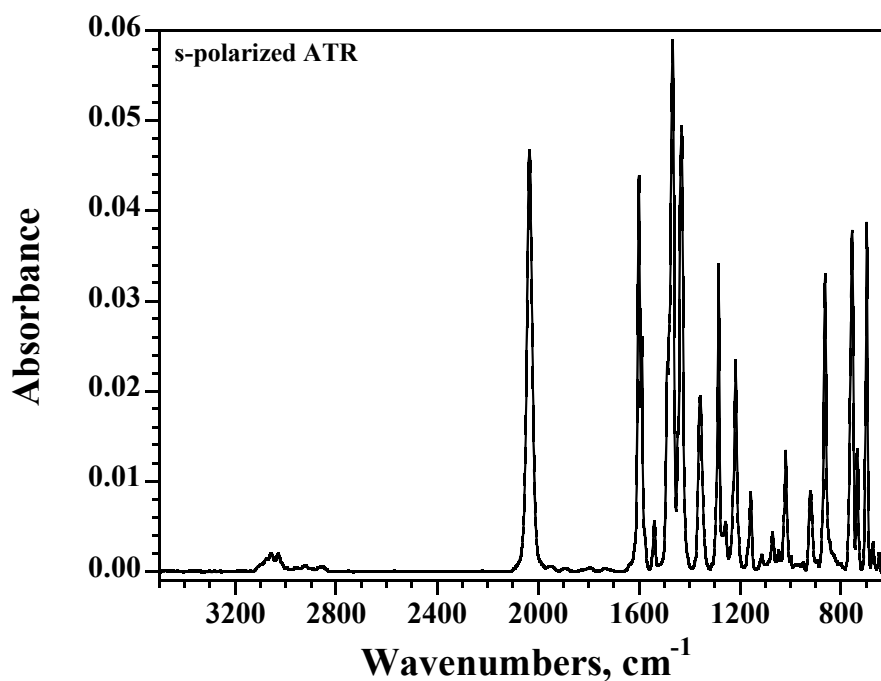


**Figure S2.** S-polarized ATR infrared spectrum of **RuapNCS**.

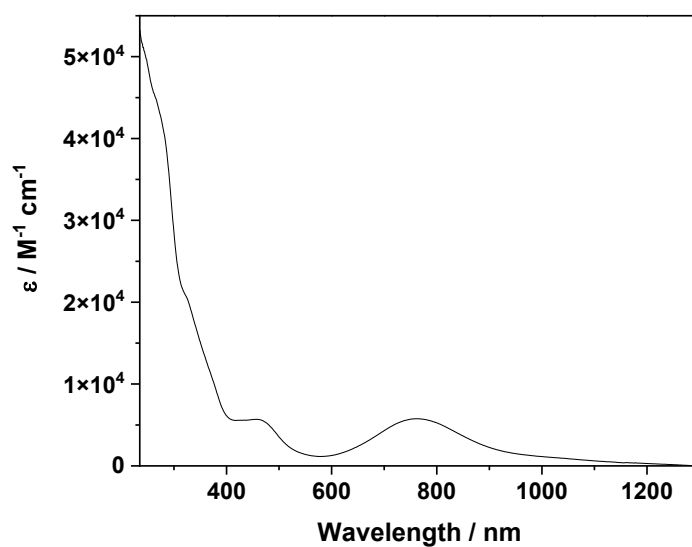


**Figure S3.** Electronic spectrum of a  $\sim 10^{-5}$  M dichloromethane solution of **RuapNCS**.

**Table S1.** Tentative assignment of the most relevant absorption bands (nm) of **RuapNCS**.

Transition/complex	RuapNCS
$\pi(\text{L}) \rightarrow \pi^*(\text{L})$	$\sim 275$ sh
$\pi(\text{N})/\delta^*(\text{Ru}_2) \rightarrow \pi^*(\text{aryl})$	$\sim 325$ sh
$\pi(\text{Ru}_2) \rightarrow \pi^*(\text{N})/\delta^*(\text{Ru}_2)$	$\sim 465$ sh
$\pi(\text{Ru-N}) \rightarrow \delta^*(\text{Ru}_2)$	770

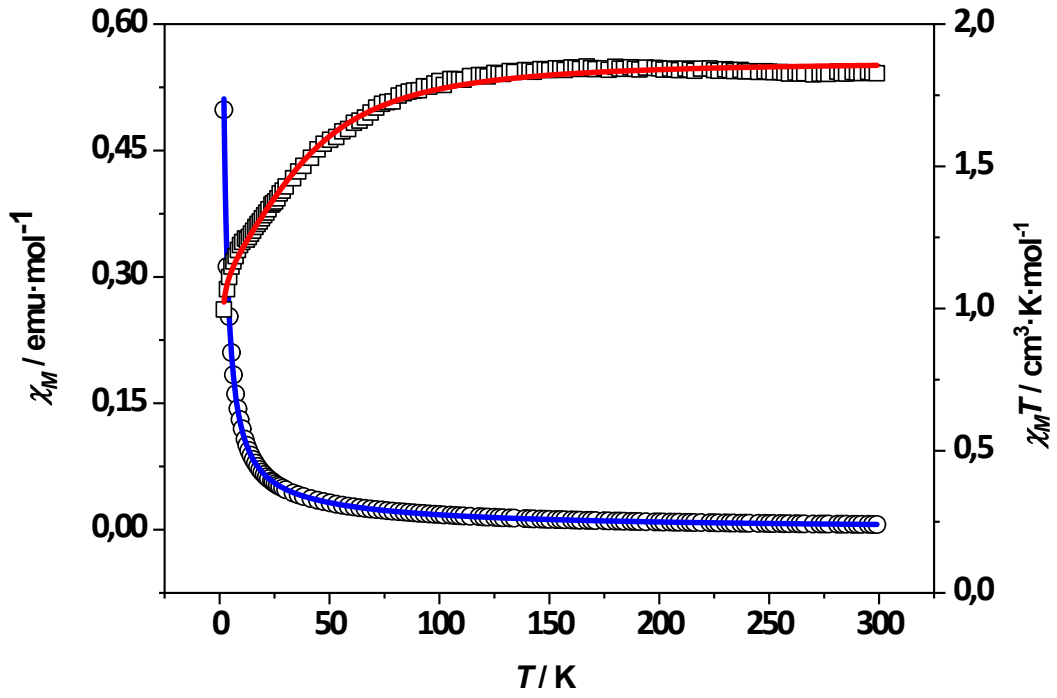


**Figure S4.** Temperature dependence of the molar susceptibility  $\chi_M$  (circles) and  $\chi_M T$  (squares) for **RuapNCS**. Solid lines are the best fit to the data using the following equations:

$$\chi_M = \frac{\chi_{\parallel} + 2\chi_{\perp}}{3}$$

Equation S1

$$\chi_{\parallel} = \left( \frac{Ng^2\beta^2}{k_B T} \right) \left[ \frac{1 + 9\exp\left(-2D/k_B T\right)}{4\left(1 + \exp\left(-2D/k_B T\right)\right)} \right]$$

Equation S2

$$\chi_{\perp} = \left( \frac{Ng^2\beta^2}{k_B T} \right) \left[ \frac{4 + \left(\frac{3k_B T}{D}\right)\left(1 - \exp\left(-2D/k_B T\right)\right)}{4\left(1 + \exp\left(-2D/k_B T\right)\right)} \right]$$

Equation S3

$$\chi_M' = \frac{\chi_M}{1 - \left(\frac{2zJ}{Ng^2\beta^2}\right)\chi_M}$$

Equation S4

( $N$ ,  $g$ ,  $\beta$ , and  $k_B$  have their usual meanings)

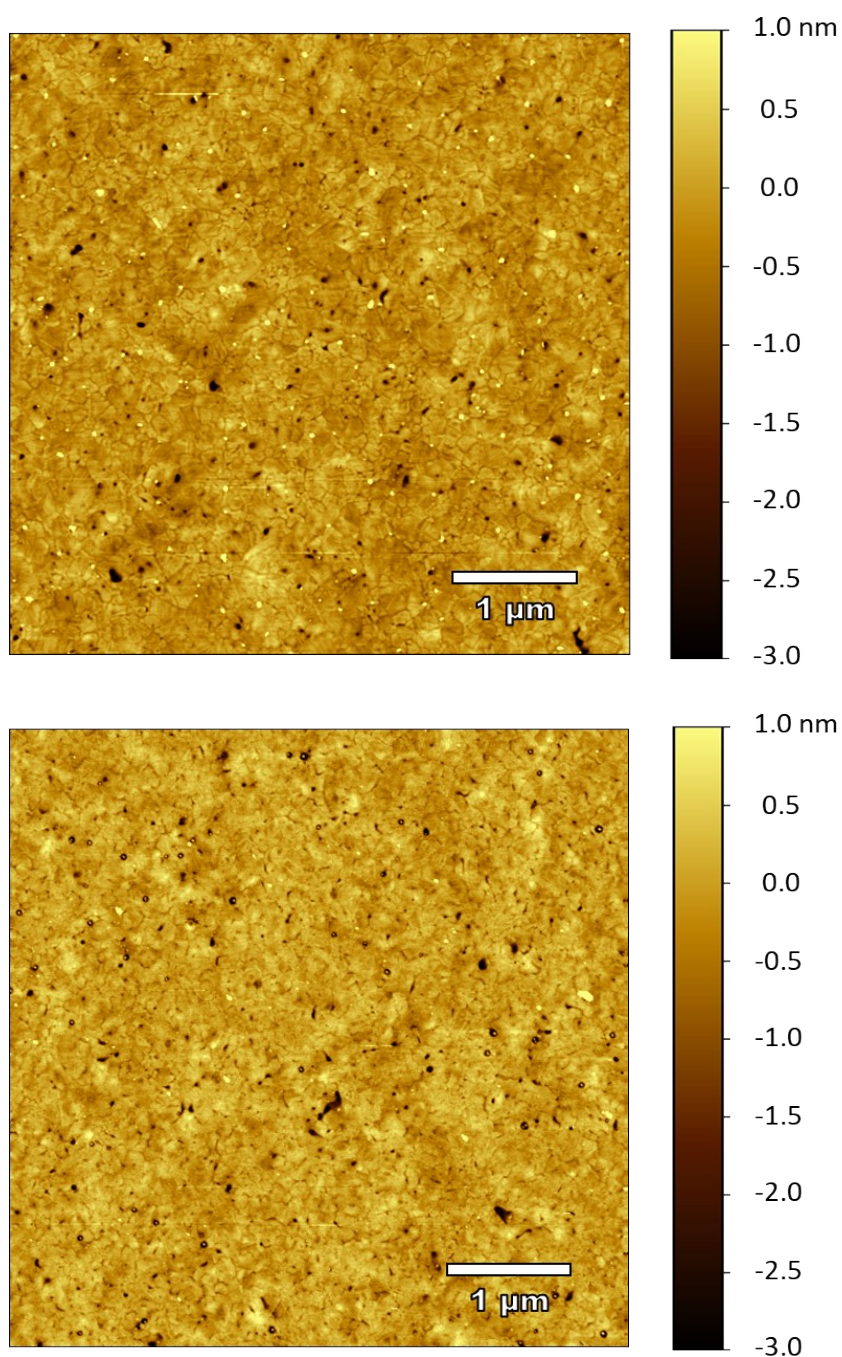


**Figure S5.** Tapping-mode AFM topography image for a blank Au<sup>TS</sup> substrate (top) and for Au<sup>TS</sup>-RuapCl (bottom).

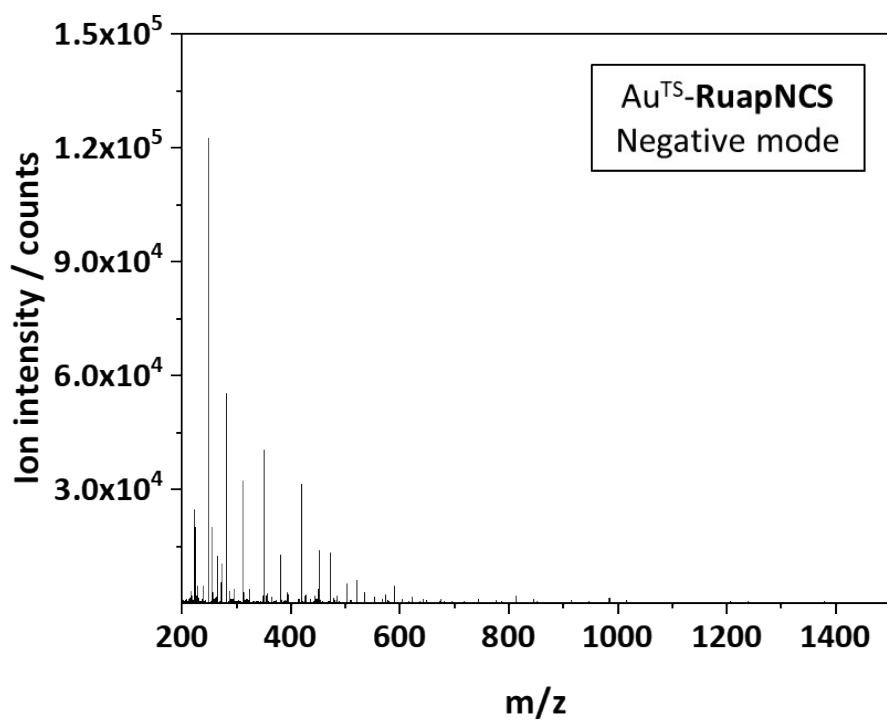
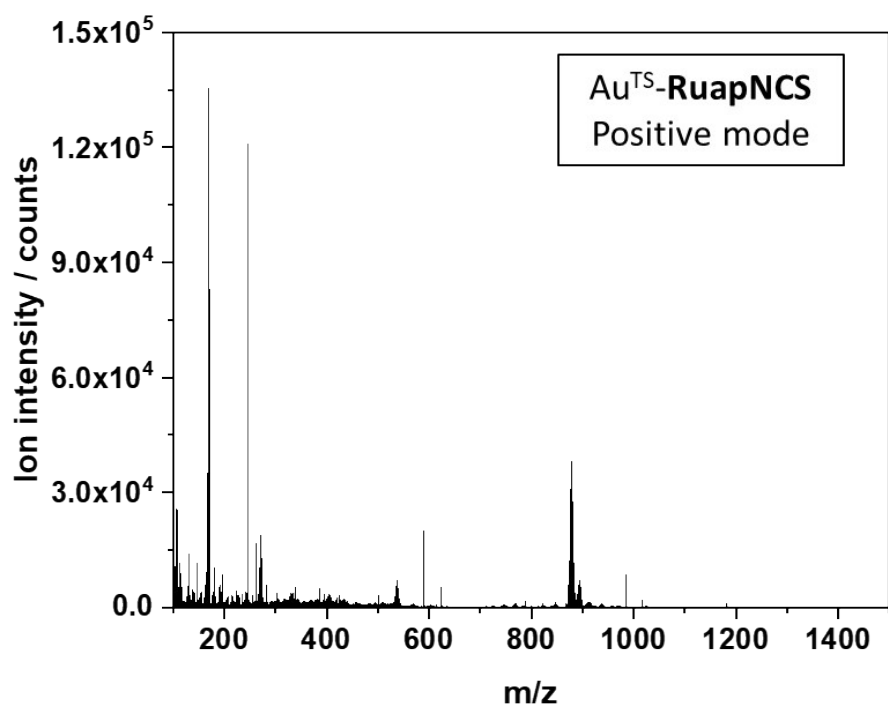


**Figure S6.** ToF-SIMS spectrum of ions derived from Au-RuapNCS in positive (top) and negative (bottom) modes.

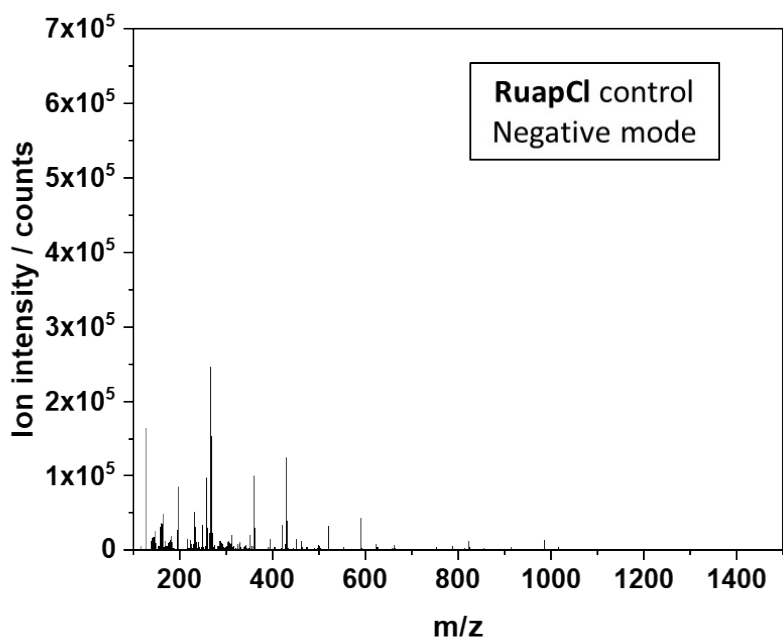
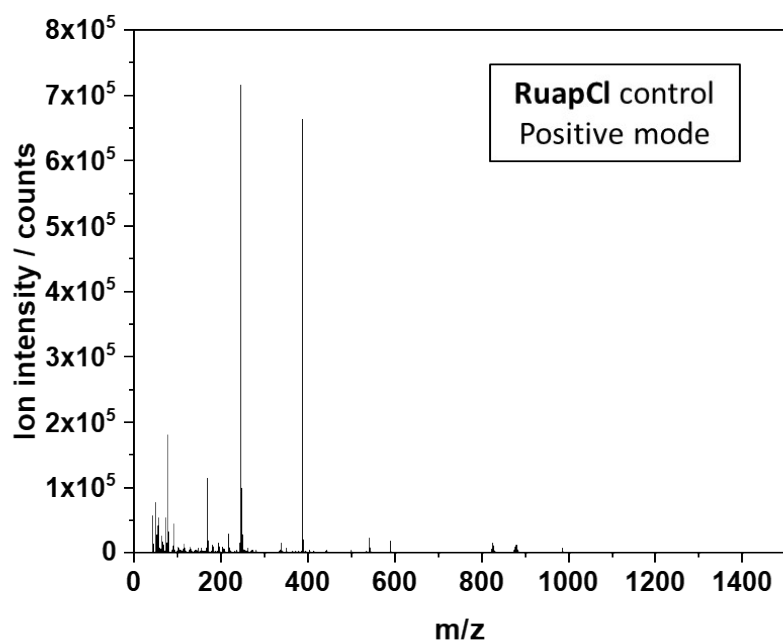


**Figure S7.** ToF-SIMS spectrum of ions derived from Au-RuapCl in positive (top) and negative (bottom) modes.

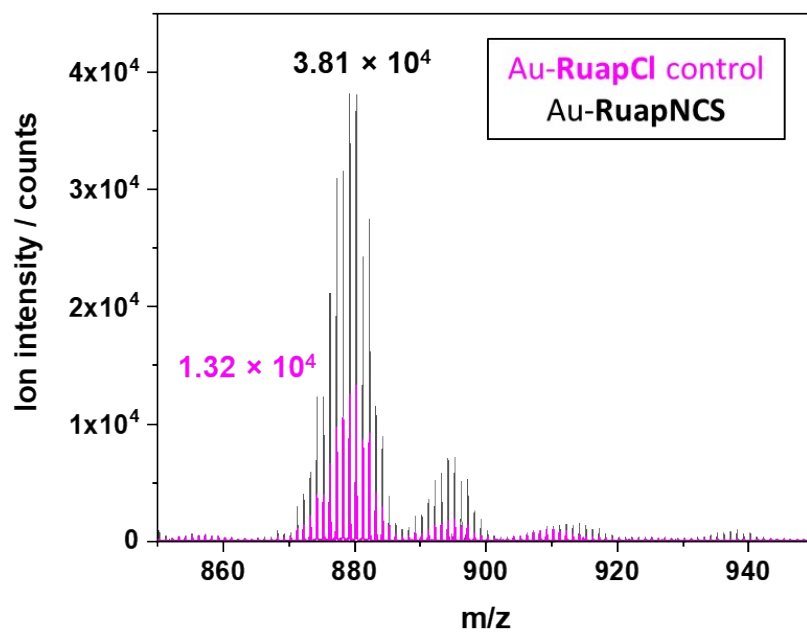


**Figure S8.** Comparison of the positive ToF-SIMS spectrum of the  $[M-X]^+$  ions for the control sample Au-RuapCl and the monolayers Au-RuapNCS.

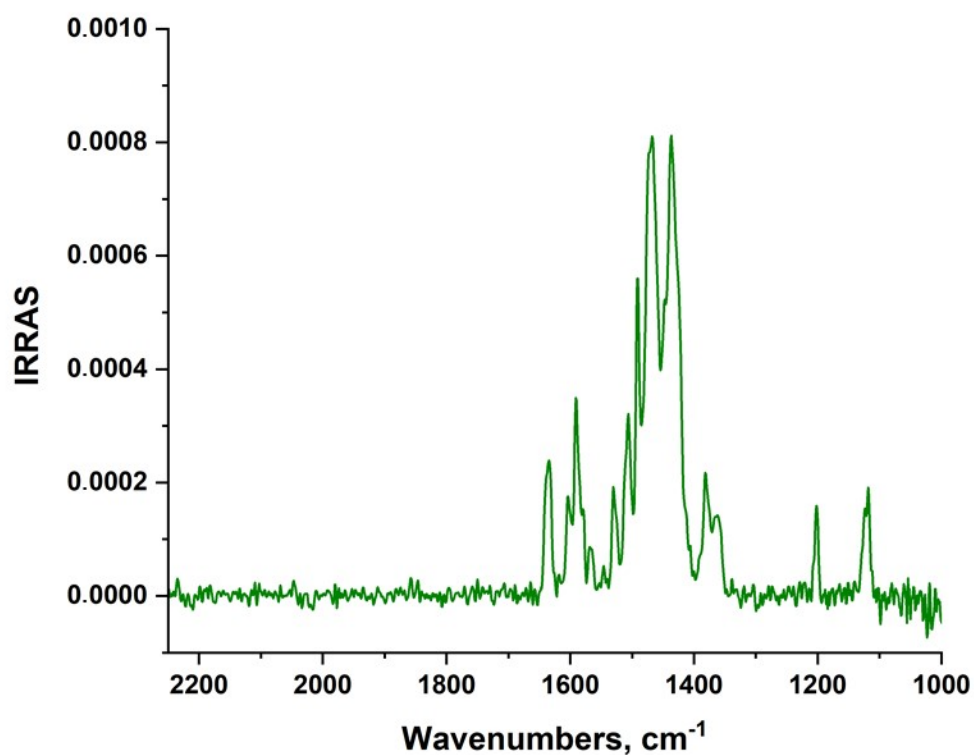


**Figure S9.** PM-IRRAS spectrum for the control sample Au-RuapCl.

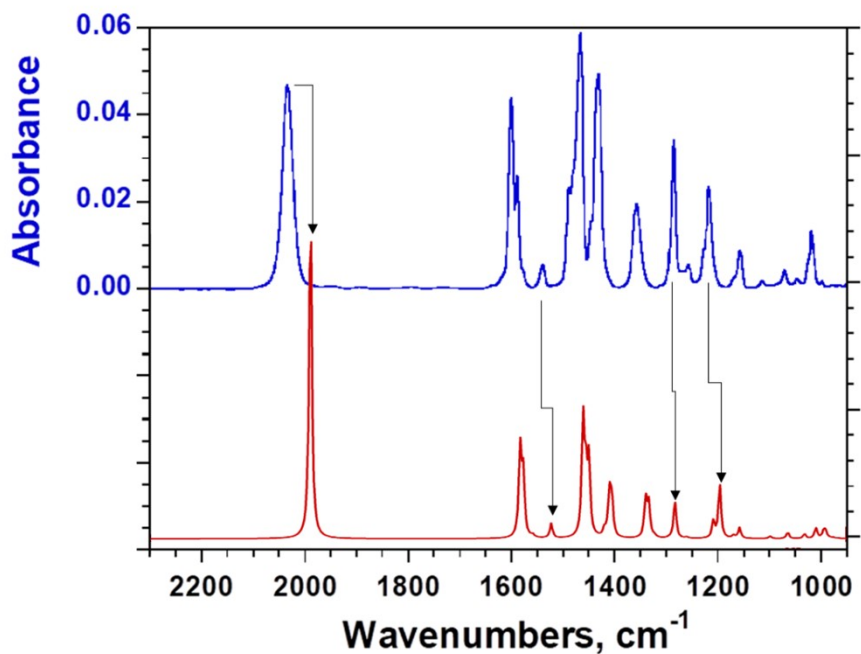


**Figure S10.** Comparison between experimental and calculated IR absorbance spectra. The correspondence between theory and experiment is indicated with an arrow for the modes used for the orientation analysis.

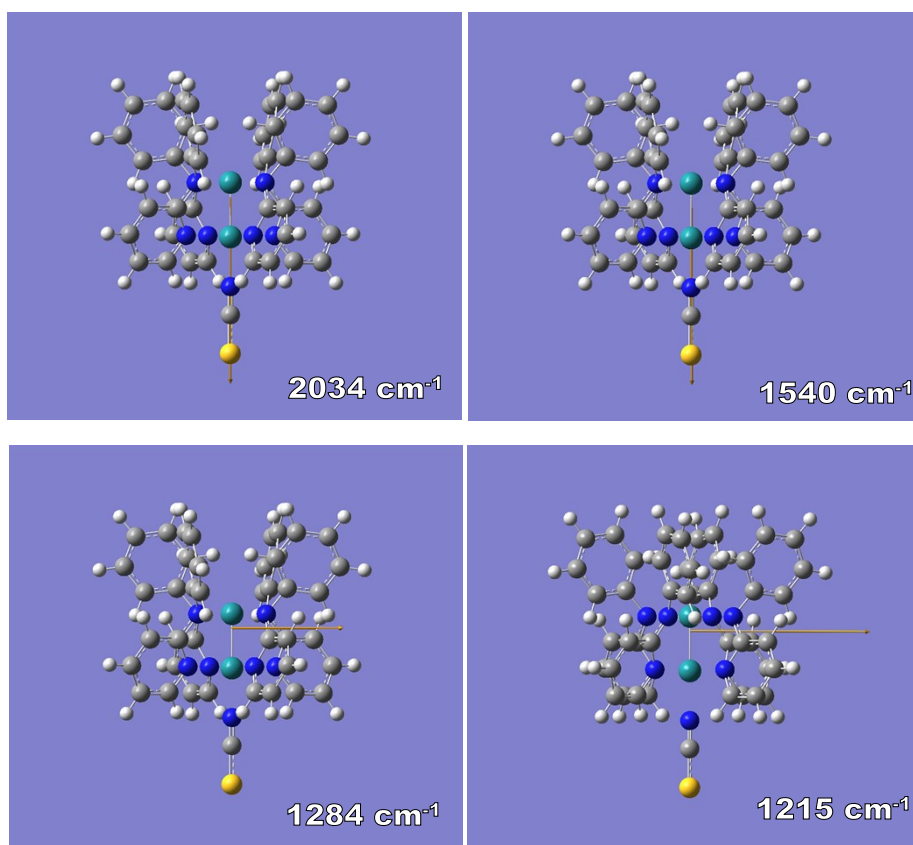


**Figure S11.** Illustration of the transition dipole vectors for the vibrational modes used for the orientation analysis in the SAMs. The reported energies correspond to the experimental values.

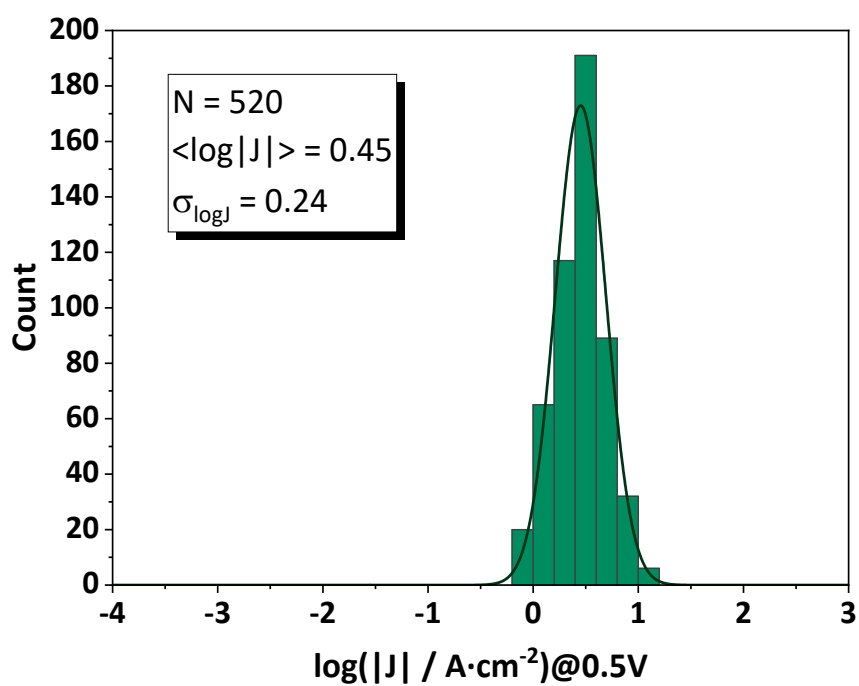
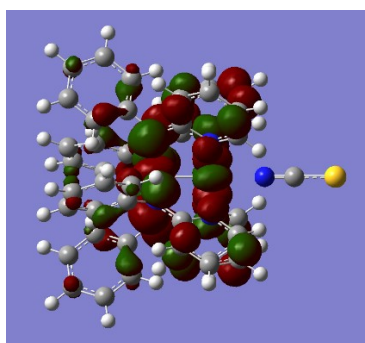
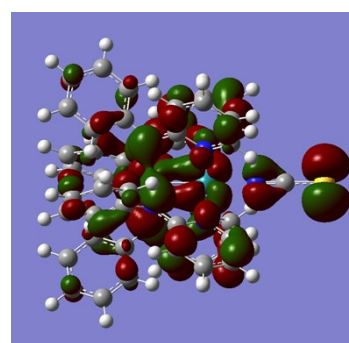


**Figure S12.** Histogram showing the distribution of  $\log |J|$  values at  $V = +0.5$  V across Au<sup>TS</sup>-RuapNCS//Ga<sub>2</sub>O<sub>3</sub>/EGaIn junctions.



Highest occupied alpha orbital



Highest occupied beta orbital

**Figure S13.** Representation of the highest occupied alpha and beta molecular orbitals from DFT calculations.

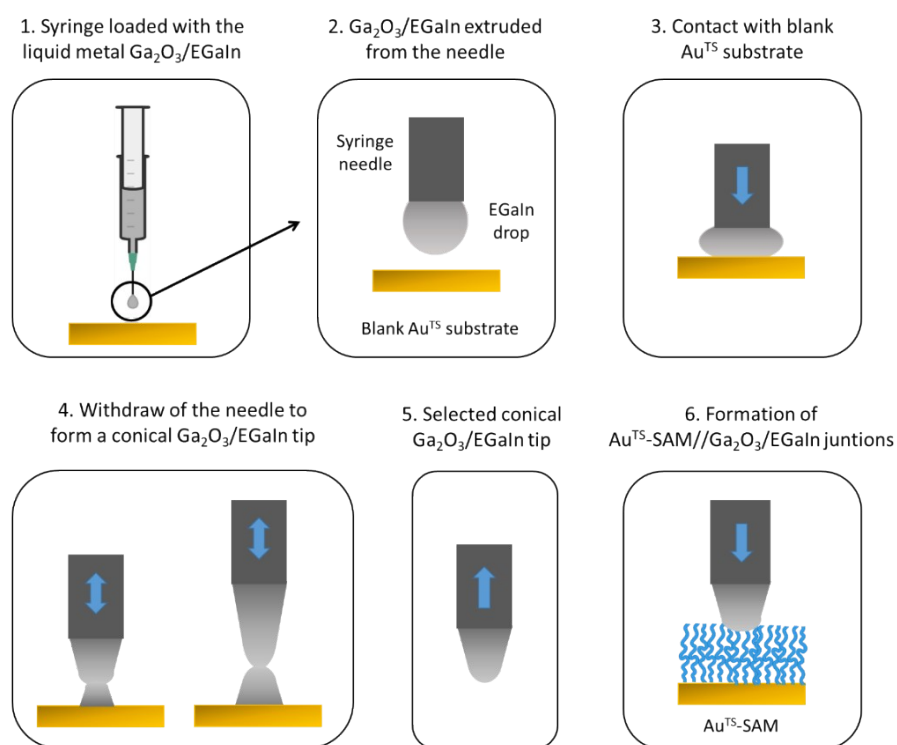


**Figure S14.** Schematics of the protocol used to prepare EGaIn conical tips and their use to measure EGaIn/Ga<sub>2</sub>O<sub>3</sub>//SAM/Au<sup>TS</sup> junctions.

## References

- (1) Chakravarty, A. R.; Cotton, F. A.; Tocher, D. A. Syntheses, Molecular Structures, and Properties of Two Polar Diruthenium(II,III) Complexes of 2-Hydroxypyridine and 2-Anilinopyridine. *Inorg. Chem.* **1985**, *24* (2), 172–177. <https://doi.org/10.1021/ic00196a011>.
- (2) Vogel, N.; Zieleniecki, J.; Köper, I. As Flat as It Gets: Ultrasoother Surfaces from Template-Stripping Procedures. *Nanoscale* **2012**, *4* (13), 3820. <https://doi.org/10.1039/c2nr30434a>.
- (3) Buffeteau, T.; Desbat, B.; Turlet, J. M. Polarization Modulation FT-IR Spectroscopy of Surfaces and Ultra-Thin Films: Experimental Procedure and Quantitative Analysis. *Appl. Spectrosc.* **1991**, *45* (3), 380–389. <https://doi.org/10.1366/0003702914337308>.
- (4) Buffeteau, T.; Desbat, B.; Blaudez, D.; Turlet, J. M. Calibration Procedure to Derive IRRAS Spectra from PM-IRRAS Spectra. *Appl. Spectrosc.* **2000**, *54* (11), 1646–1650. <https://doi.org/10.1366/0003702001948673>.
- (5) Ramin, M. A.; Le Bourdon, G.; Daugey, N.; Bennetau, B.; Vellutini, L.; Buffeteau, T. PM-IRRAS Investigation of Self-Assembled Monolayers Grafted onto SiO<sub>2</sub>/Au Substrates. *Langmuir* **2011**, *27* (10), 6076–6084. <https://doi.org/10.1021/la2006293>.
- (6) Frisch, M. J.; Trucks, G. W.; Schlegel, H. B.; Scuseria, G. E.; Robb, M. A.; Cheeseman, J. R.; Scalmani, G.; Barone, V.; Mennucci, B.; Petersson, G. A.; Nakatsuji, H.;

Caricato, M.; Li, X.; Hratchian, H. P.; Izmaylov, A. F.; Bloino, J.; Zheng, G.; Sonnenberg, J. L.; Hada, M.; Ehara, M.; Toyota, K.; Fukuda, R.; Hasegawa, J.; Ishida, M.; Nakajima, T.; Honda, Y.; Kitao, O.; Nakai, H.; Vreven, T.; Montgomery, J. A.; Peralta, J. E.; Ogliaro, F.; Bearpark, M.; Heyd, J. J.; Brothers, E.; Kudin, K. N.; Staroverov, V. N.; Kobayashi, R.; Normand, J.; Raghavachari, K.; Rendell, A.; Burant, J. C.; Iyengar, S. S.; Tomasi, J.; Cossi, M.; Rega, N.; Millam, J. M.; Klene, M.; Knox, J. E.; Cross, J. B.; Bakken, V.; Adamo, C.; Jaramillo, J.; Gomperts, R.; Stratmann, R. E.; Yazyev, O.; Austin, A. J.; Cammi, R.; Pomelli, C.; Ochterski, J. W.; Martin, R. L.; Morokuma, K.; Zakrzewski, V. G.; Voth, G. A.; Salvador, P.; Dannenberg, J. J.; Dapprich, S.; Daniels, A. D.; Farkas; Foresman, J. B.; Ortiz, J. V.; Cioslowski, J.; Fox, D. J.; Montgomery J. A., Jr.; Peralta, J. E.; Ogliaro, F.; Bearpark, M.; Heyd, J. J.; Brothers, E.; Kudin, K. N.; Staroverov, V. N.; Kobayashi, R.; Normand, J.; Raghavachari, K.; Rendell, A.; Burant, J. C.; Iyengar, S. S.; Tomasi, J.; Cossi, M.; Rega, N.; Millam, N. J.; Klene, M.; Knox, J. E.; Cross, J. B.; Bakken, V.; Adamo, C.; Jaramillo, J.; Gomperts, R.; Stratmann, R. E.; Yazyev, O.; Austin, A. J.; Cammi, R.; Pomelli, C.; Ochterski, J. W.; Martin, R. L.; Morokuma, K.; Zakrzewski, V. G.; Voth, G. A.; Salvador, P.; Dannenberg, J. J.; Dapprich, S.; Daniels, A. D.; Farkas, Ö.; Foresman, J. B.; Ortiz, J. V.; Cioslowski, J.; Fox, D. J. *Gaussian 09, Revision A.1*; Gaussian, Inc.: Wallingford, CT, 2009.

(7) <https://cccbdb.nist.gov/vsfx.asp>.